International Journal of Thermofluids 7–8 (2020) 100046

Contents lists available at ScienceDirect

International Journal of Thermofluids

journal homepage: www.elsevier.com/locate/ijtf

Spectral method solutions of a variable aspect ratio duct flow in a uniform transverse magnetic field with two different thermal boundary conditions

Mohammed Al-Khawaja[a,*], Mohamed Selmi[b]

[a] Department of Mechanical and Industrial Engineering, Qatar University, Qatar
[b] Qatar General Electricity & Water Corporation (KAHRAMAA), Qatar

ARTICLE INFO

Article History:
Received 16 May 2020
Revised 17 September 2020
Accepted 17 September 2020
Available online 25 September 2020

Keywords:
Rectangular duct flow
MHD flow
MFM flow
Liquid metal
Electrically conducted fluid
Spectral method
Aspect ratio
Chebyshev polynomials

ABSTRACT

A laminar electrically-conducting flow inside an electrically-insulated rectangular duct in a uniform transverse magnetic field with both uniform surface temperature and uniform heat flux boundary conditions are considered numerically. The problem with aspect ratios of the range from 1:10 to 10:1 and Hartmann number M up to 1000 is solved using a highly accurate technique which is spectral method. The flow variables are expanded in terms of linear combinations of Chebyshev polynomials chosen to satisfy the boundary conditions implicitly. The resulting equations are collocated using the Gauss points to produce a system of nonlinear algebraic equations which is solved iteratively using Gauss elimination. Convergence properties of the numerical method reveals that for aspect ratio of less than 4 to 1, the flow is well resolved with as small as 29 by 29 Chebyshev polynomials; however, as the aspect ratio increases to more than 4 to 1, the number of polynomials required for an adequate resolution can be as high as 49 by 49 polynomials. It is found when the magnetic field is turned on, the pressure drop, in general, increases with the field for different aspect ratios. However, the pressure drop increase will be slower near the aspect ratio of 10. Also, the heat transfer increases with the field for most of the cases, but for some cases the field will have adverse effect on the heat transfer, particularly, for constant surface temperature boundary condition at aspect ratio > 4 and $M < 100$. On the other hand, this effect will be noticed at aspect ratio > 4 and $M < 10$ for uniform wall heat flux boundary condition.

1. Introduction

Due to its importance and vast applications (such as MHD pumps, MHD generators, MHD flow meters, MHD nuclear fusion reactor, MHD marine propulsion, MHD stirring of molten metal and magnetic-levitation casting, etc.), the magneto-hydrodynamics has become the primary interests for many researchers since last century.

Sayed-Ahmed [1] has solved numerically the problem of MHD flow and heat transfer in a rectangular duct with constant wall heat flux axially and constant wall temperature peripherally. He examined the effect of the Hall term and the variable viscosity on the velocity and temperature fields.

Smolentsev [2,3] studied experimentally laminar heat transfer in MHD-flow in a rectangular duct with large aspect ratio, 10:1, for the case of one-sided heating with the heat flux applied to one of the side walls. He has found experimentally and numerically that the correlation of the fully-developed temperature distribution in the channel cross-section with the magnetic field occurs in a certain range only at relatively small Hartmann numbers. As the Hartmann number increases within that range the temperature at the channel centerline decreases.

Sai [4] has examined analytically the effects of suction or injection on an incompressible laminar flow in a rectangular duct with non-conducting walls in the presence of an imposed transverse magnetic field. He used the solutions for the velocity and magnetic field to obtain the current density and electric field strength.

Verardi [5] has presented, using finite element method, the full solution of a three-dimensional steady magnetohydrodynamic flow with moderately high Hartmann numbers and interaction parameters. An incompressible, viscous and electrically conducting liquid-metal is considered. Results are presented for Hartmann numbers in the range 10^2–10^3.

Kumamaru [6] has preformed three-dimensional numerical calculations on liquid-metal magnetohydrodynamic flow through a rectangular channel in the inlet region of the applied magnetic field, including a region upstream the magnetic field section. Along the flow axis (i.e. the channel axis), the pressure decreases slightly as normal non- MHD flow, increases once, thereafter decreases sharply and finally decreases

* Corresponding author.
E-mail addresses: khawaja@qu.edu.qa (M. Al-Khawaja), mselmi@km.qa (M. Selmi).

https://doi.org/10.1016/j.ijft.2020.100046

Nomenclature

a	Rectangle width [m]
B_0	Uniform magnetic flux [T]
b	Rectangle length [m]
D_h	Hydraulic diameter [m]
f	Friction factor
H	Dimensionless induced axial magnetic field, $H_z/[V_m(\sigma\mu_f)^{1/2}]$
H_z	Induced axial magnetic field [A/m]
H^*	Normalized induced axial magnetic field, H/γ
h_c	Heat-transfer coefficient [w/m^2·°C]
k	Thermal conductivity of fluid [w/m·°C]
M	Hartmann number, $B_0D_h(\sigma/\mu_f)^{1/2}$
Nu	Nusselt number, h_cD_h/k
p	Fluid pressure [N/m^2]
q	Surface heat flux [W/m^2]
Re	Reynolds number, V_mD_h/ν
r	Aspect ratio, a/b
T_s	Surface temperature [°C]
T	Temperature [°C]
V_m	Mean axial velocity [m/s]
V_z	Axial fluid velocity [m/s]
w	Dimensionless axial velocity, V_z/V_m
w^*	Negative normalized axial velocity, w/γ
x	x-coordinate [m]
x^*	Dimensionless x-coordinate, x/a
y	y-coordinate [m]
y^*	Dimensionless y-coordinate, y/a
z	Axial coordinate [m]

Greek Letters

γ	Non-dimensional pressure gradient, $[(\partial p/\partial z)(D_h{}^2)]/V_m\mu_f$
∇^2	Laplacian in dimensionless rectangular coordinate
θ	Dimensionless temperature, $(T-T_s)/(D_hq/k)$
θ_m	Mean dimensionless temperature defined in Eq. (10)
μ_f	Dynamic viscosity of fluid [N·s/m^2]
ν	Kinematic viscosity of fluid, m^2/s
ρ	Density of fluid [kg/m^3]
σ	Electrical conductivity of fluid [A/V·m]

Subscripts

c	Refers to convection
f	Refers to friction
h	Refers to hydraulic
m	Refers to mean
z	Refers to component in z-direction
s	Refers to surface

as fully-developed MHD flow. The sharp decrease in the pressure, resulting in a large pressure drop, in the inlet region is due to increase in the induced electric current in this region comparing with that in the fully-developed region. In the inlet region, the flow velocity distribution changes from a parabolic profile of a laminar non-MHD flow to a flat profile of a fully developed MHD flow.

Nesliturk [7] used a stabilized finite element with the residual-free bubble (RFB) functions to solve the resulting governing equations from MHD flow in a rectangular duct for the case when the flow is driven by the current produced by electrodes, placed one in each of the walls of the duct where the applied magnetic field is perpendicular. He assumed flow is steady, laminar and the fluid is incompressible, viscous and electrically conducting. He depicted the changes in direction and intensity with respect to the values of wall inductance in terms of level curves for both the velocity and the induced magnetic field.

Bozkaya [8] derived a fundamental solution for the coupled convection-diffusion type equations. He employed the boundary element method (BEM) application then, established with this fundamental solution, for solving the coupled equations of steady MHD duct flow in the presence of an external oblique magnetic field. Then he solved MHD duct flow problems with the most general form of wall conductivities and for large values of Hartmann number. The results, he obtained, for velocity and induced magnetic field is visualized in terms of graphics for values of Hartmann number $M = < 300$.

Using highly accurate numerical method (i.e. spectral method), Al-Khawaja and Selmi [9] have solved the magneto-fluid-mechanic square problem with heat transfer. The modified Navier-Stokes and the non-linear energy equations were solved to get the pressure drop and Nusselt problem for low and very high Hartmann number M (= 1000).

For circular cross-section with uniform surface heat flux, the MHD problem of free-and-forced convection flow was solved numerically using the modified third-accurate-upwind scheme developed by Al-Khawaja and Agarwal [10] to stabilize the solution resulted from highly non-linear equations. The solutions were so interesting since the velocity profiles have a shape of valleys and hills and it varies with Hartmann number. Also, the appearance of the temperature contours looks like fish-mouth shape.

Li, Sutevski, Smolentsev, and Abdou [11] have studied the same problem numerically and experimentally but under non-uniform transverse magnetic field. They have found that the pressure distributions, in the duct cross sections for two different sections of the liquid metal flow at the entry to and at the exit from the magnet, are different. Also, MHD flow of liquid metal through a right angled isosceles triangular duct has been studied by Sarma and Deka [12] numerically. They have solved for the velocity, induced magnetic field and temperature distributions using 9-point stencil centered finite difference method for different values of Hartmann number, Magnetic Reynold number and Prandtl number.

In recent years, there are quite numbers of papers which have been published on MHD flows inside a duct with and without heat transfer. For examples, high-resolution direct numerical simulations were conducted by Dmitry Krasnov, Oleg Zikanov and Thomas Boeck [13] to analyze turbulent states of flow of an electrically conducting fluid in a duct of square cross-section with electrically insulating walls and imposed transverse magnetic field. The Reynolds number of the flow is 10^5 and the Hartmann number varies from 0 to 400. It was found that there is a broad range of Hartmann numbers in which the flow is neither laminar nor fully turbulent, but has laminar core, Hartmann boundary layers and turbulent zones near the walls parallel to the magnetic field. Also, MHD flow equations in a rectangular duct in the presence of transverse external oblique magnetic field were solved by Ibrahim Çelik [14] using Chebyshev polynomial method. Numerical solutions of velocity and induced magnetic field were obtained for steady-state, fully developed, incompressible flow for a conducting fluid inside the duct. The results for velocity and induced magnetic field were visualized in terms of graphics for values of Hartmann numbers. Later, the mixed convection in a downward flow in a vertical duct with strong transverse magnetic field was studied numerically by Xuan Zhang and Oleg Zikanov [15] and it was found that the flow is steady-state or oscillating depending on the strengths of the heating and magnetic field. Moreover, C. N. Kim [16] studied a numerical analysis of three-dimensional liquid MHD flows in a square duct with an FCI in a non-uniform magnetic field. Detailed information on flow velocity, Lorentz force, pressure, current and electric potential of MHD duct flows for different Hartmann numbers was predicted. Additionally, the steady, laminar, fully developed MHD flow of an incompressible, electrically conducting fluid with temperature dependent viscosity was investigated by Elif Ebren Kaya and Münevver Tezer-Sezgin [17] in a rectangular duct together with its heat transfer. Although the induced magnetic field is neglected due to the small Reynolds number, the Hall

effect, viscous and Joule dissipations are taken into consideration. The momentum and the energy equations were solved iteratively. It was observed that as Hartmann number is increasing, the velocity magnitude drops which is a well-known property of the MHD duct flow and increasing viscosity parameter reduces both the flow and the temperature magnitudes whereas the increase in the Hall parameter accelerates the flow and increases the fluid temperature. Likewise, the 2D transient MHD flow in a rectangular duct in terms of the velocity of the fluid and the induced magnetic field by using the radial basis function (RBF) approximation was simulated by Münevver TEZER-SEZGİN and Merve GÜRBÜZ [18]. It was shown that, as Hartmann number increases, the fluid becomes stagnant at the center of the duct, the flow is flattened and boundary layers are developed on the Hartmann and side walls. Stable solutions were obtained with RBF by using quite large time increment and suitable relaxation parameters on the expense of explicit Euler time-integration scheme used.

MHD flows with different geometries have been studied by many researchers recently. For examples, Sultan Z. Alamri [19] has investigated the effects of mass transfer on MHD second grade fluid towards stretching cylinder. It was noted that the velocity increases with increasing values of fluid parameter whereas it declines for the case of magnetic field. Finally, it was demonstrated numerically by Z H. Khan [20] for flow with heat transfer in a trapezoidal cavity that the imposed magnetic field, thermal buoyancy, porous medium permeability and the length of the heating element play a crucial role in the enhancement of dimensionless average heat transfer rate.

In the present work, the spectral method solutions of a variable aspect ratio rectangular duct flow in a uniform transverse magnetic field with uniform surface temperature and uniform surface heat flux thermal boundary conditions have been studied. The range of the aspect ratio used is from 0.1 to 10 while the range of Hartmann number M is taken from 0 (no magnetic field) to 1000 (very high magnetic field). It was noticed the pressure drop, in general, increases with the field for different aspect ratios. However, the pressure drop increase will be slower when the aspect ratio becomes high. Also, the heat transfer increases with the magnetic field for most of the cases, but for some cases the field will have adverse effect on the heat transfer, particularly, for constant surface temperature boundary condition at aspect ratio $>$ 4 and $M < 100$. On the other hand, this effect will be noticed at aspect ratio $>$ 4 and $M < 10$ for uniform wall heat flux boundary condition.

2. Basic Equations

The modified Navier-Stokes equations which include the effect of the magnetic field body force were derived and discussed in references [9,10]. Also, the energy equation was shown in these references. Here, the simplified dimensionless basic equations of heated MFM flow in rectangular coordinates (shown in Fig. 1), for steady, incompressible, fully-developed flow, are derived and given as

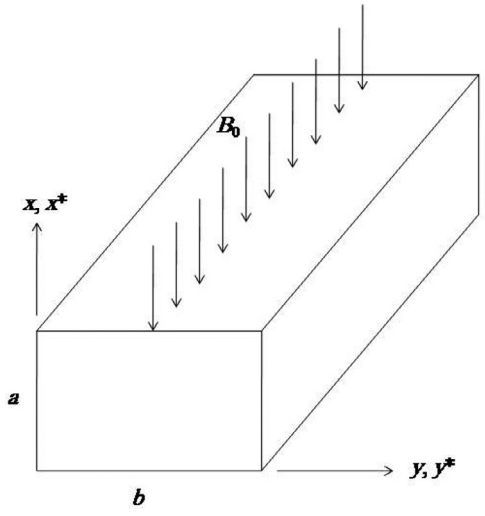

Fig. 1. Problem geometry which shows the transverse magnetic field along a rectangular duct flow.

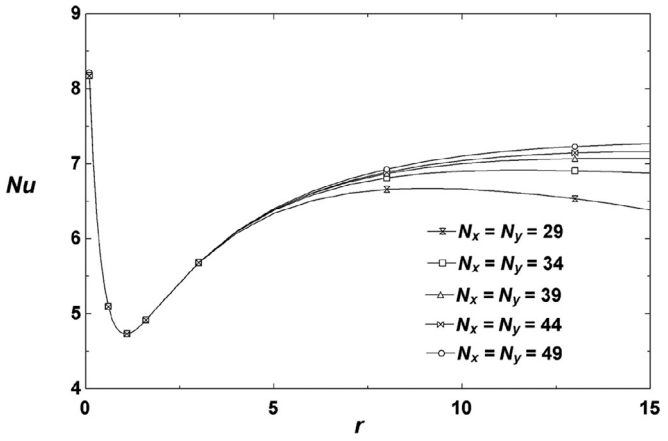

Fig. 2. Computed Nusselt number versus aspect ratio for different resolution for $M = 1000$ with the case of constant wall temperature.

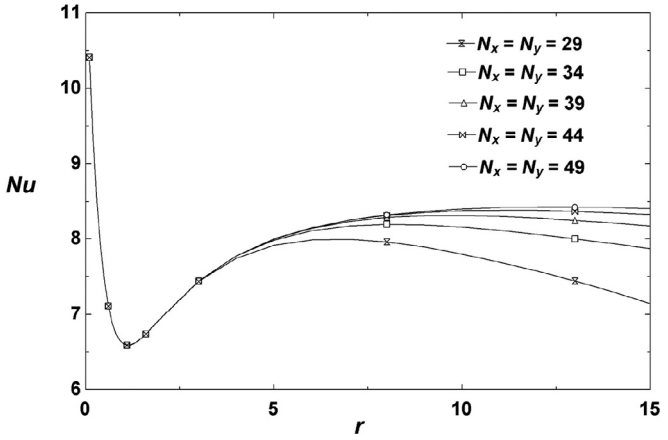

Fig. 3. computed Nusselt number versus aspect ratio for different resolution for $M = 1000$ with the case of constant wall heat flux.

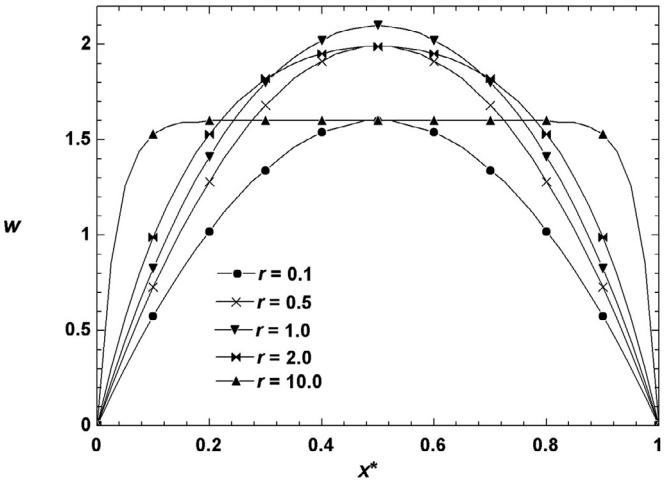

Fig. 4. Dimensionless axial velocity profiles across the duct (at the mid-point of the side along y direction) in the direction of the magnetic field for different aspect ratios at $M = 0$.

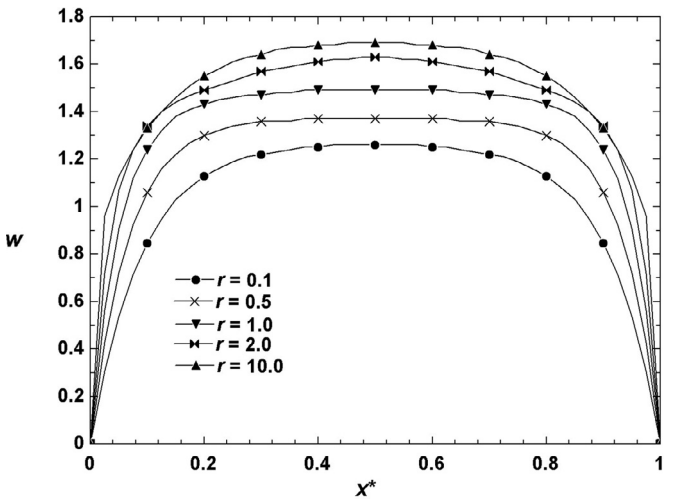

Fig. 5. Dimensionless axial velocity profiles across the duct (at the mid-point of the side along *y* direction) in the direction of the magnetic field for different aspect ratios at $M = 20$.

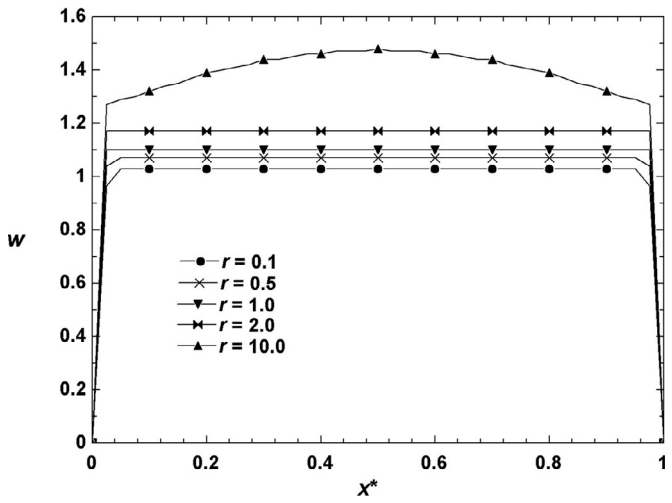

Fig. 6. Dimensionless axial velocity profiles across the duct (at the mid-point of the side along *y* direction) in the direction of the magnetic field for different aspect ratios at $M = 200$.

following:

$$\nabla^2 w^* - \frac{1}{2}(r+1)M\frac{\partial H^*}{\partial x^*} = 1 \tag{1}$$

$$\nabla^2 H^* - \frac{1}{2}(r+1)M\frac{\partial w^*}{\partial x^*} = 0 \tag{2}$$

$$\nabla^2\theta + (r+1)^2 Nu\, w\theta = 0 \tag{3}$$

and

$$\nabla^2\theta - 2(r+1)w = 0 \tag{4}$$

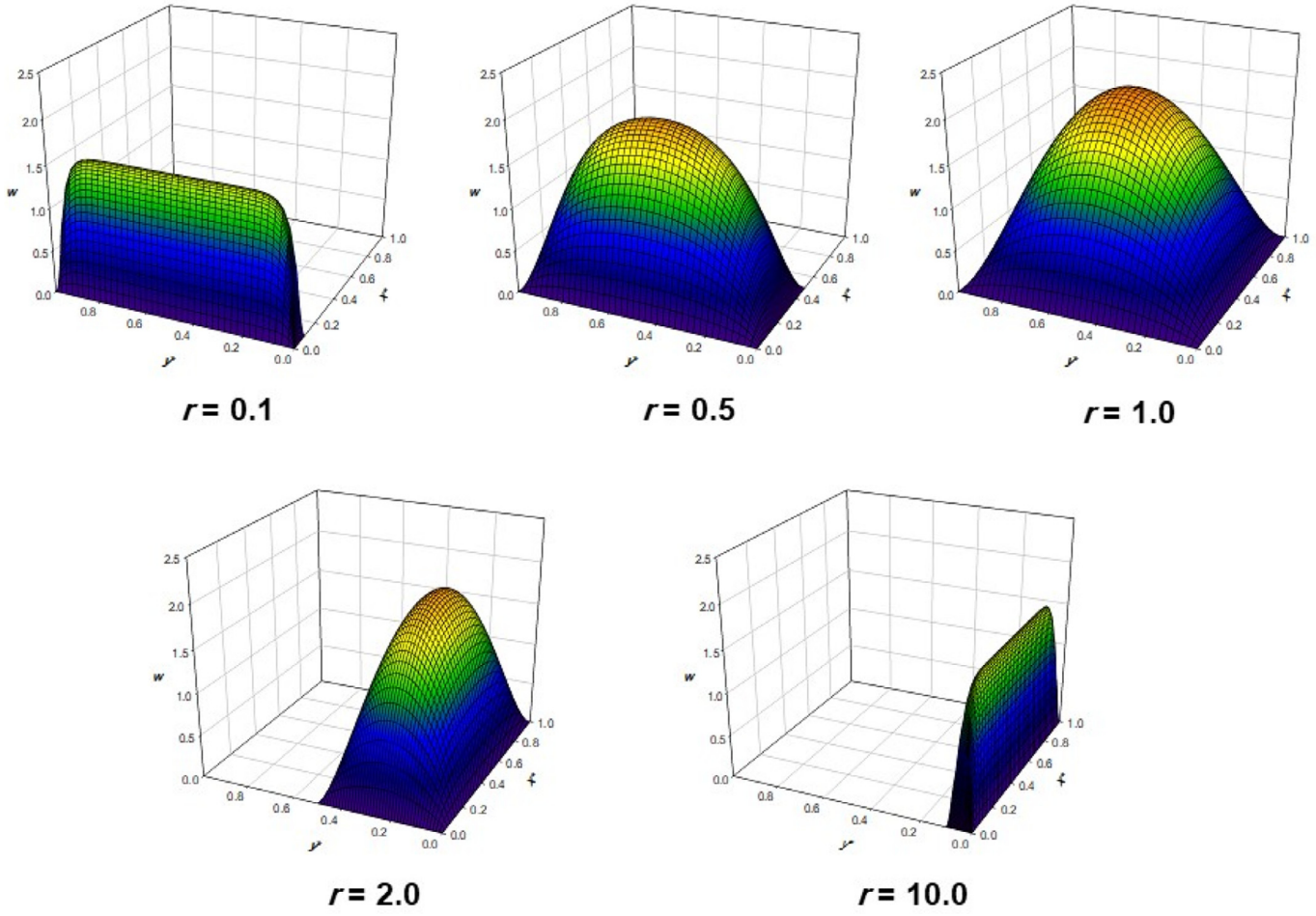

Fig. 7. 3-D mesh of the dimensionless axial velocity profiles at $M = 0$ for different aspect ratios.

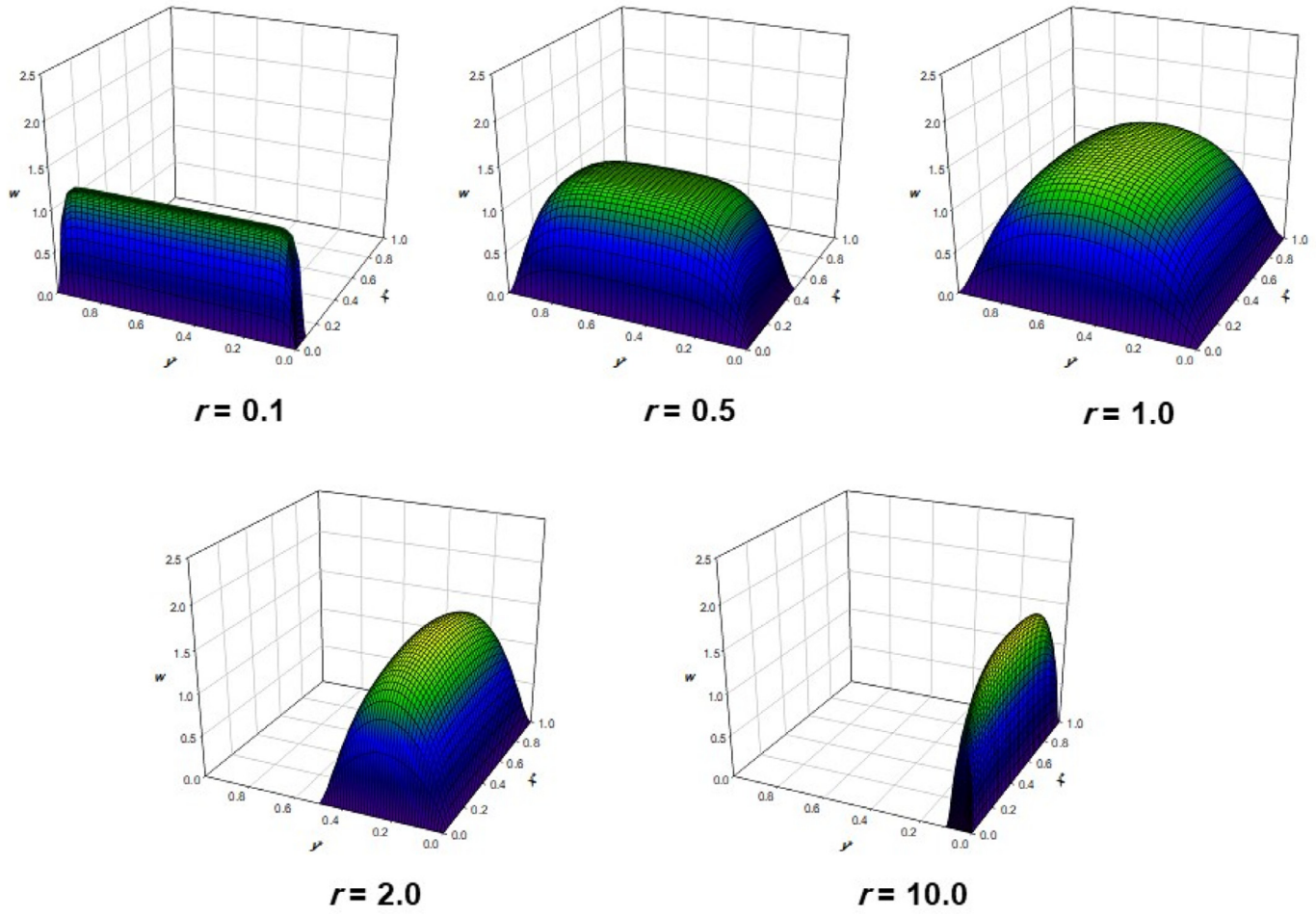

Fig. 8. 3-D mesh of the dimensionless axial velocity profiles at $M = 20$ for different aspect ratios.

Where the negative dimensionless pressure gradient γ is related to w^* by

$$\gamma = \frac{1/r}{\int_0^{1/r}\int_0^1 w^* dx^* dy^*} \tag{5}$$

Equations (1) and (2) represent the axial momentum and induction, respectively, whereas (3) and (4) represent the energy equations for uniform surface temperature and uniform heat flux boundary conditions, respectively. Cleary, one can notice the aspect ratio $r = a/b$ enters all governing equations and makes them to represent the general rectangular cross section. If r is equal to unity, the special case of square cross section will be obtained and the simplified equations for this case are given in reference [9].

From the force balance one can show that $fRe = -8\gamma/(r+1)^2$ while from Nu definition, one can also show that $Nu = -2/[\theta_m(r+1)]$. Where the mean dimensionless temperature is given by

$$\theta_m = \frac{\int_0^{1/r}\int_0^1 \theta w dx^* dy^*}{\int_0^{1/r}\int_0^1 w dx^* dy^*} \tag{6}$$

Definitions of other dimensionless variables are described in the notation section. The boundary conditions are $w^* = 0$ (from no-slip condition), $H^* = 0$ (from electrically insulated surface), and $\theta = 0$.

3. Numerical Method

The flow variables can be approximated by the following expansion functions made of linear combinations of Chebyshev polynomials

$$w^* = \sum_{m=0}^{N_x-1}\sum_{n=0}^{N_y-1} C_{mn}^w X_m^w(\tilde{x}) Y_n^w(\tilde{y}) \tag{7}$$

$$H^* = \sum_{m=0}^{N_x-1}\sum_{n=0}^{N_y-1} C_{mn}^H X_m^H(\tilde{x}) Y_n^H(\tilde{y}) \tag{8}$$

$$\theta = \sum_{m=0}^{N_x-1}\sum_{n=0}^{N_y-1} C_{mn}^\theta X_m^\theta(\tilde{x}) Y_n^\theta(\tilde{y}) \tag{9}$$

where

$$\tilde{x} = 2x^* - 1; \ldots \tilde{y} = 2ry^* - 1$$

are algebraic mappings that transform the cross-section of the duct into the domain of Chebyshev polynomials, $(\tilde{x}, \tilde{y}) \in [-1, 1] \times [-1, 1]$; $X_m^w, X_m^H, X_m^\theta, Y_n^w, Y_n^H$, and Y_n^θ are linear combinations of Chebyshev polynomials, chosen to satisfy the boundary conditions implicitly,

$$X_m^w(\tilde{x}) = X_m^\theta(\tilde{x}) = T_{km+2}(\tilde{x}) - T_{km}(\tilde{x}) \tag{10}$$

$$X_m^H(\tilde{x}) = T_{k(m+1)+1}(\tilde{x}) - T_{k(m+1)-1}(\tilde{x}) \tag{11}$$

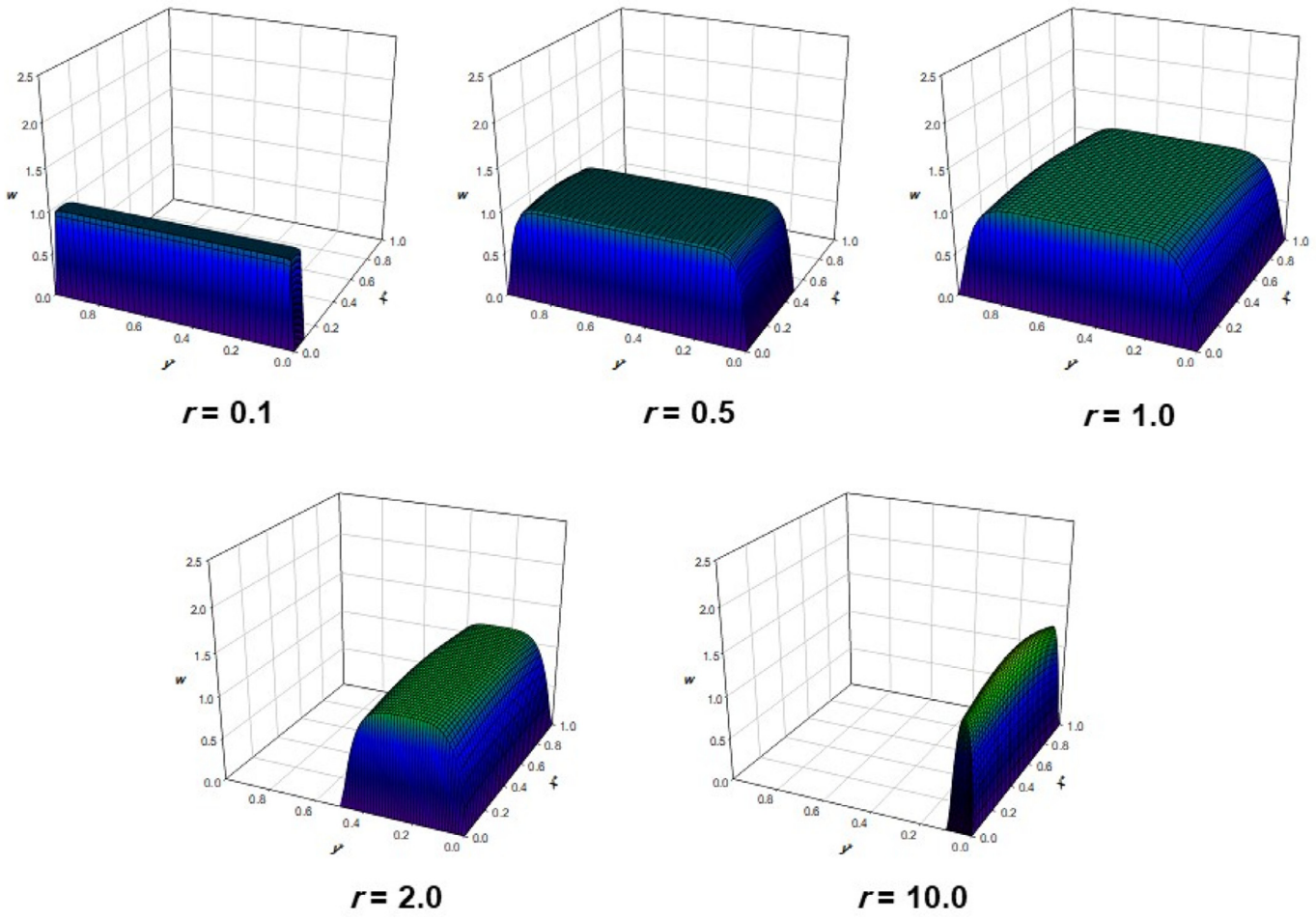

Fig. 9. 3-D mesh of the dimensionless axial velocity profiles at $M = 200$ for different aspect ratios.

$$Y_n^w(\tilde{y}) = Y_n^\theta(\tilde{y}) = T_{kn+2}(\tilde{y}) - T_{kn}(\tilde{y}) \tag{12}$$

$$Y_n^H(\tilde{y}) = T_{kn+2}(\tilde{y}) - T_{kn}(\tilde{y}) \tag{13}$$

Here k can take on the values of either 1 or 2. If $k = 2$, symmetry is exploited, that is even Chebyshev polynomials are selected for$w^*$and θ in both the x, y directions; while even polynomials are selected for H^*in the y direction and odd ones are chosen in the x direction. This reduces computational time as the computational domain is reduced to one quadrant; $(\tilde{x}, \tilde{y}) \in [0,1] \times [0,1]$. If $i = 1$, no symmetry is exploited and the solution is sought on the whole domain.

The spectral solution presented here is divided into two parts. First Eqs. (1) and (2) are solved simultaneously using the first two expansions, Eqs. (7) and (8), and then the energy equation, Eq. (3) or (4) depending on the problem considered, is solved as a second part using the third expansion, Eq. (9).

First, Eqs. (7) and (8) are substituted into the first two of the governing equations, Eqs. (1) and (2), and the resulting equations are

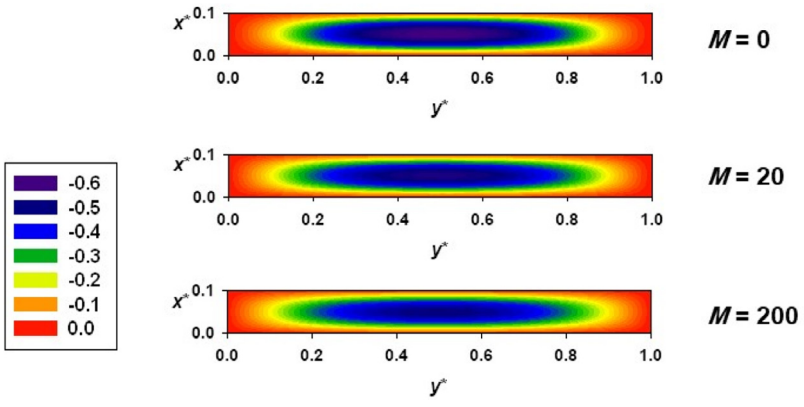

Fig. 10. Dimensionless temperature contours are shown in color bands for $r = 0.1$ and different Hartmann numbers with uniform surface temperature boundary condition.

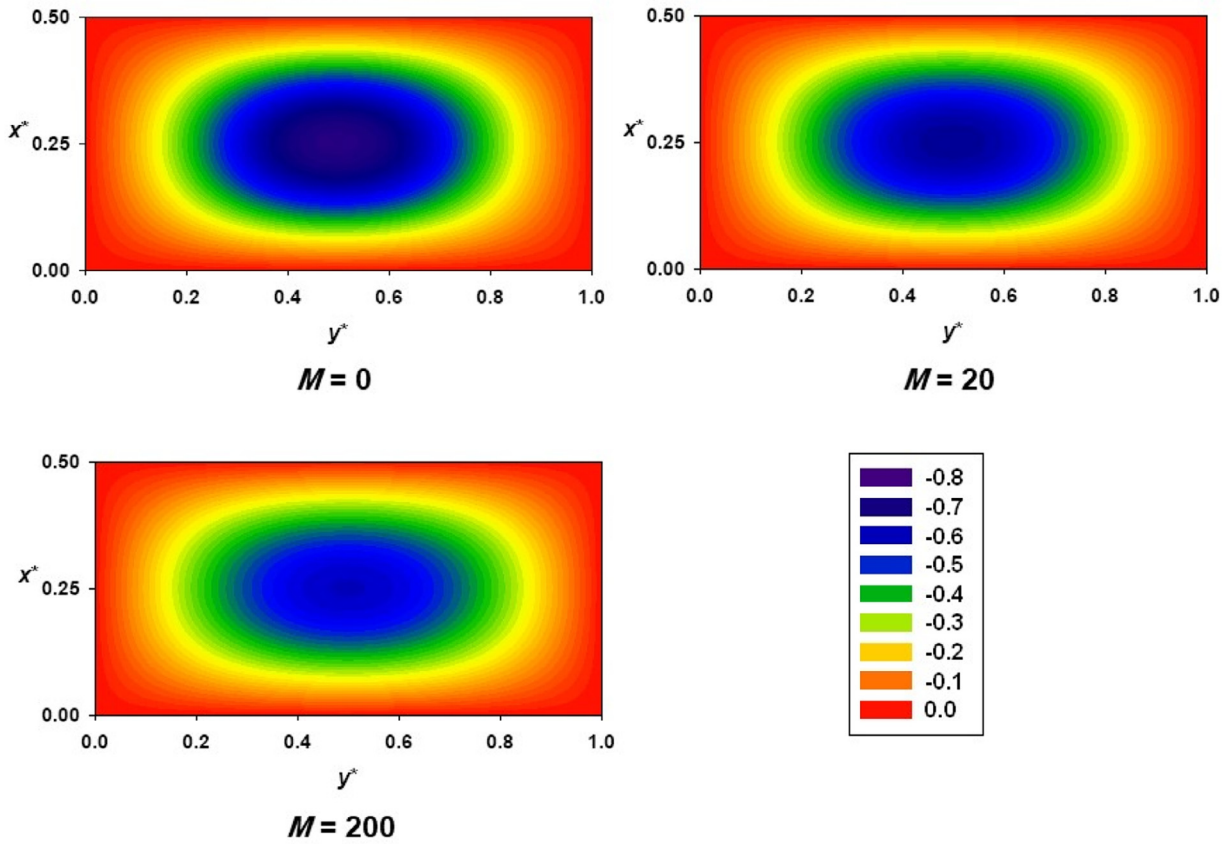

Fig. 11. Dimensionless temperature contours are shown in color bands for $r = 0.5$ and different Hartmann numbers with uniform surface temperature boundary condition.

satisfied at the Gauss points:

$$\left(\tilde{x}_i, \tilde{y}_j\right) = \left(\cos\frac{(2i+1)\pi}{2N_x k}, \cos\frac{(2j+1)\pi}{2N_y k}\right) \tag{14}$$

where $i = 0,1,2,\ldots, N_x - 1$ and $j = 0,1,2,\ldots, N_y - 1$. The resulting system of algebraic equations is written symbolically as

$$\mathbf{f}(\mathbf{C}; M) = 0 \tag{15}$$

Where **C** is a vector of size $N = 2N_xN_y$containing the expansion coefficients C^w_{mn} and C^H_{mn} and **f** is a vector-valued function also of size N that contains the discrete form of Eqs. (1) and (2). Equation (15) represents a linear system of algebraic equations and is solved by Gauss elimination to yield the coefficients C^w_{mn} and C^H_{mn} from which the velocity $w^*$and normalized magnetic field $H^*$are computed through Eqs. (7) and (8).

Second, Eq. (3) is solved iteratively while Eq. (4) is solved directly. For Eq. (3), once $w^*$is known, γ can be computed from Eq. (5); however, θ_m and consequently Nu cannot be computed from Eq. (6) alone. As a result, a guessed value for Nu is first assumed and then Eq. (3) is solved by substituting the expansion, Eq. (9), into Eq. (3) and the resulting equation is satisfied at the collocation points, Eq. (14). This yields a system of N algebraic equations that is solved for the approximate coefficients of θ, i.e. C^θ_{mn}. Once an approximation to θ is obtained, a more accurate value of Nu can be obtained from Eq. (6) and another approximation to θ is sought again by solving Eq. (3) using the new value of Nu. This process is repeated till successive approximations become within a small relative error from each other. For Eq. (4), no iteration is required as it does not contain Nu and therefore by simply substituting the expansion for θ, Eq. (9), into the energy equation, Eq. (4) and applying the collocation scheme defined by Eq. (14) a linear algebraic system is obtained that is solved for the expansion coefficients of θ. Figures 2 and 3 show the computed Nusselt number versus the aspect ratio for different resolution for $M = 1000$ with the case of constant wall temperature and uniform wall heat flux, respectively. The figures indicate that with aspect ratios of up to 4 a resolution of 29×29 is acceptable for $M = 1000$ while for aspect ratio beyond 4 a higher resolution is required, i.e. 49×49. The solutions that have been worked out here have been computed with a resolution of 49×49 in order to achieve adequate accuracy of the numerical solutions even for $M < 1000$.

4. Results and Discussion

The special case of square cross section was solved numerically [9,21,22]. The fluid mechanics part as well the heat transfer one either with uniform surface temperature or uniform surface heat flux were considered and compared with circular cross section case. In this paper, a more general case is investigated, i.e. a rectangular cross section with different aspect ratios. Very interesting results, which will be discussed later, are obtained. The aspect ratio is varied from 0.1 to 10 while Hartmann number M is varied from 0 (no magnetic field) to 1000 (very high magnetic field).

The geometry of this problem is shown in Fig. 1. The magnetic field is directed vertically in the negative x direction while the flow is directed in the positive z direction.

As a first test, the dimensionless axial velocity w along the magnetic field direction is plotted, at the midpoint with y direction. Fig. 4 shows the velocity for $M = 0$ (that is conventional flow) versus x^* for different aspect ratios. As expected, the square duct will have a

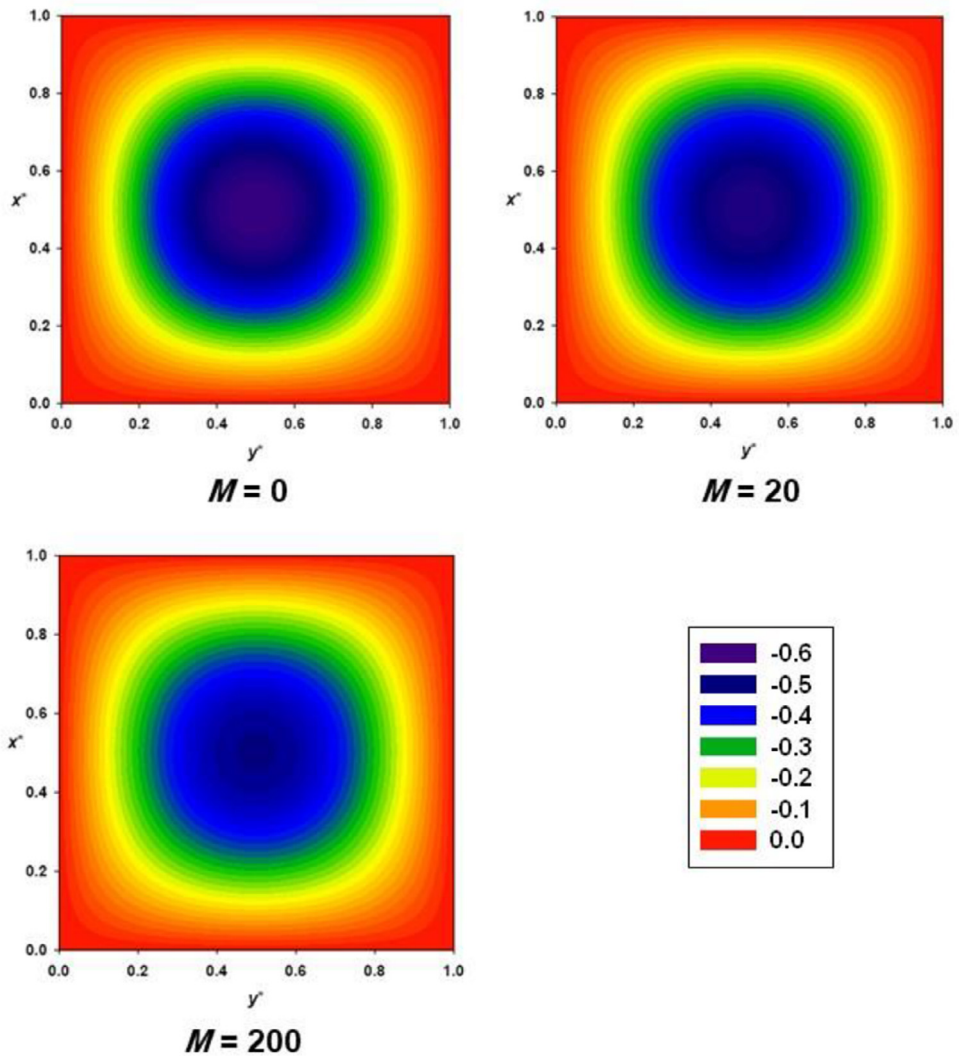

Fig. 12. Dimensionless temperature contours are shown in color bands for $r = 1$ (i.e. square) and different Hartmann numbers with uniform surface temperature boundary condition.

velocity profile parabolic shape whereas it will be disturbed for other aspect ratios, particularly for $r = 10$. At this ratio, the profile will be mostly flat along the duct with x direction and it will have steep gradient near the surfaces. This is also true for $r = 0.1$ along the duct with y direction (shown later in 3-D plot, Fig. 7). The reason of this behavior is that when $r = 10$, for example, the length in x direction will be larger by 10 times than that for y direction. Thus, the viscous effect in y direction will be smaller than that for the other direction. This will make the profile in x direction flatter while the other will be round. For other aspect ratios ($0.1 < r < 10$), the viscous effect on the profile shape will be in between.

Those profiles will be disturbed completely when the magnetic field is turned on. Due to Hartmann effect, all the profiles will be flattened along the magnetic field. However, the profile corresponds to $r = 10$, is less flattened and its value becomes the highest due to the fact that the short length in the y direction is exposed slightly by the magnetic field. This is shown in Figs. 5 and 6 for low Hartmann number ($M = 20$) and high Hartmann number ($M = 200$), respectively. The well-known flattening of the profiles is more noticeable for high Hartmann number and the thin Hartmann boundary layer is formed for all aspect ratios except for $r = 10$ where the profile will be somehow round over most of the cross section of the duct for the same reason mentioned above.

The 3-D plots of the velocity profiles describe clearly what was mentioned above. Figs. 7, 8, and 9 show 3-D mesh of the dimensionless velocity profiles for $M = 0$, $M = 20$, and $M = 200$, respectively with different aspect ratios. Out of those profiles, the profiles with $r = 0.1$ and 10 for different Hartmann number values have an interesting behavior. For $M = 0$, the profile, as discussed above, will be almost uniform along y for $r = 0.1$ and along x for $r = 10$. However, this uniformity for the latter case will be upset for $M = 20$ and $M = 200$, as shown in Figs. 8 and 9, but for the former case the profiles will form a shape of parallelepiped, particularly, for high Hartmann number. This is because the longer side is affected by the magnetic field. The case of $r = 1$ (i.e. square cross section) was solved in references [9,21,22] and explained how the profile parallel to the field is flattened while the normal one will be more round since the effect of the pondromotive force is less on that direction.

Also, the heat transfer is affected as well by the aspect ratio and Hartmann number. This will be shown as dimensionless temperature contours with varying in color. There are two groups of these figures depending on the thermal boundary condition. The first group will be for constant surface temperature while the second one will be for uniform surface heat flux. For first group, Fig. 10 shows the contours for $r = 0.1$ with different M. One can notice that as M gets higher, the

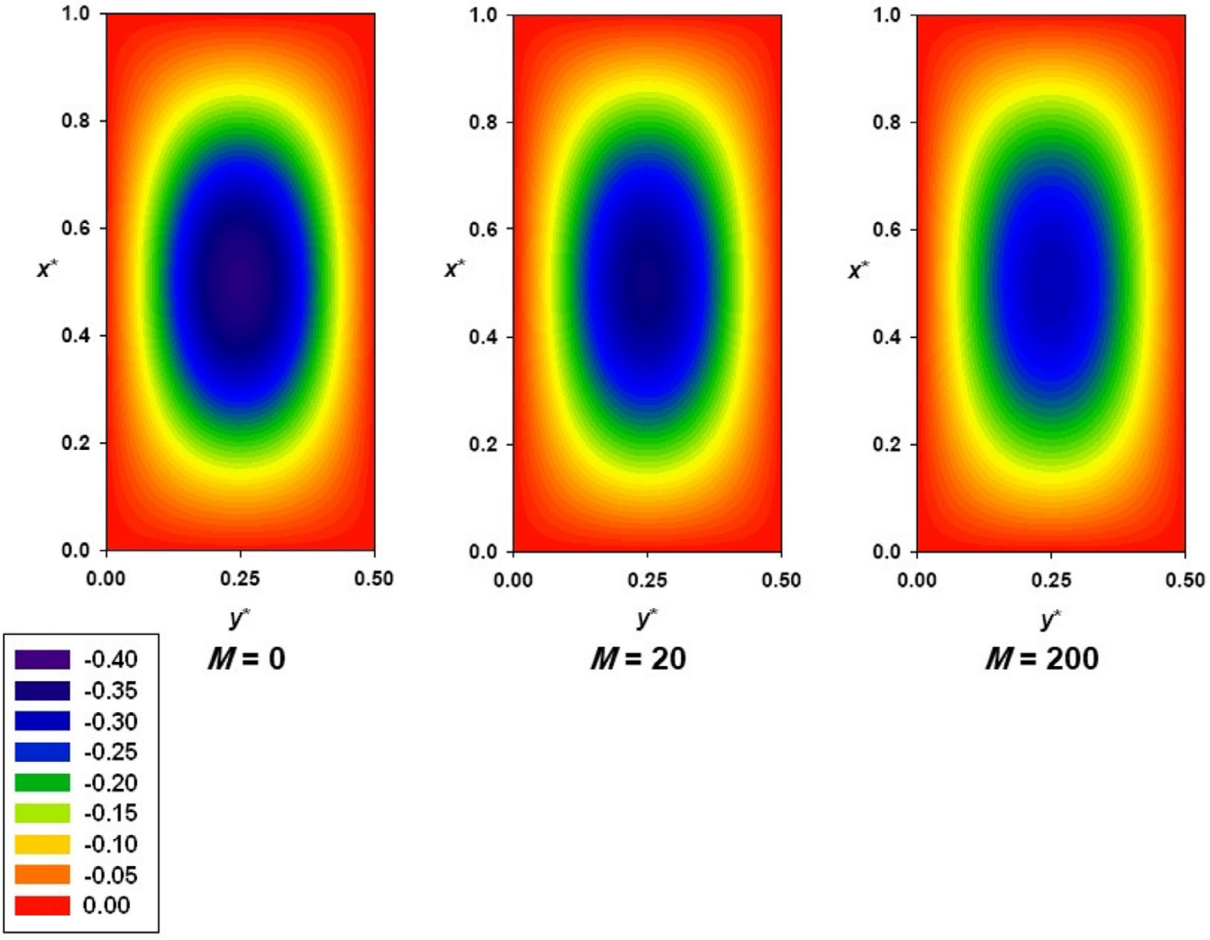

Fig. 13. Dimensionless temperature contours are shown in color bands for $r = 2$ and different Hartmann numbers with uniform surface temperature boundary condition.

uniformity of the temperature distribution across the cross section will be more obvious. This is again due the fact that the longer side is exposed to the magnetic field and thus the flow will be more affected by the field. Of course, at $M = 200$, the strong Hartmann effect also will affect the temperature distribution and make it more uniform. It will be very similar for $r = 0.5$ and $r = 1$, shown in Figs. 11 and 12. However, for $r = 2$ and $r = 10$, the behavior will start to reverse as shown in Figs. 13 and 14 and this is because the shorter side is exposed to the field and makes the duct less influenced by the field while the viscous effect will be dominant along x axis, particularly, for $r = 10$.

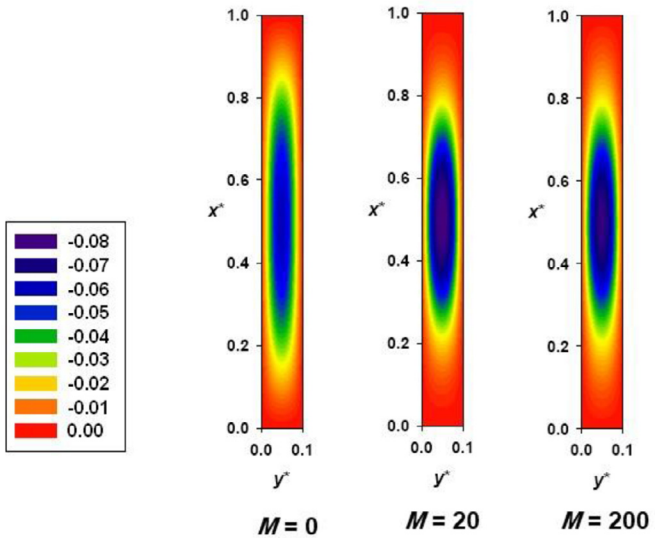

Fig. 14. Dimensionless temperature contours are shown in color bands for $r = 10$ and different Hartmann numbers with uniform surface temperature boundary condition.

The second group which illustrates the dimensionless temperature contours for constant surface heat flux is shown in Figs. 15, 16, 17 and 18 for $r = 0.1$, 0.5, 2, and 10, respectively. For all cases, the uniformity of the contours of this group is more obvious from their counterparts of the first group. As before, the magnetic field effect is to increase the regularity of the temperature distribution over the cross section, particularly for $r = 0.1$ and 0.5, but for $r = 2$ and 10, the field will not affect the homogeneity of the temperature distribution even for high Hartmann number ($M = 200$). In contrast to the constant surface temperature case, the reversal behavior with M is not noticed here. This is because the temperature distribution is more homogenous (higher Nusselt number) in the case of constant surface heat flux.

The velocity profiles and temperature contours discussed above will give some explanation of the friction behavior and heat transfer variation of the flow. The friction factor behavior is explained in Fig. 19 in which the parameter fRe is plotted against r for different values of Hartmann number. As M increases, the symmetry of the plot about $r = 1$ and at $M = 0$ will be disturbed. The lowest friction is depicted at $r = 1$ and $M = 0$. Thus, for conventional flow, the square shape will have the lowest pressure drop relative to other general

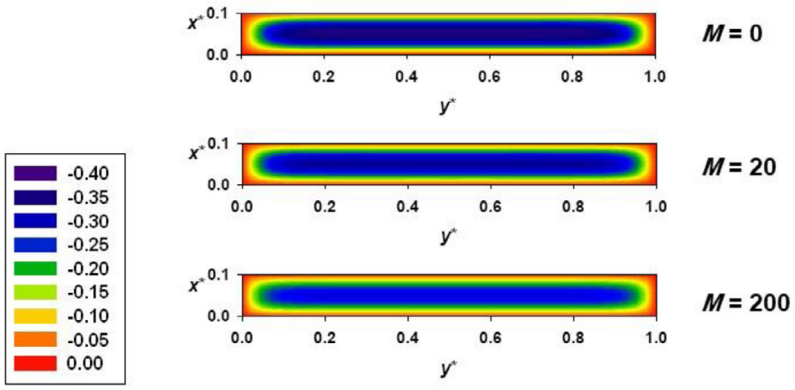

Fig. 15. Dimensionless temperature contours are shown in color bands for $r = 0.1$ and different Hartmann numbers with uniform surface heat flux boundary condition.

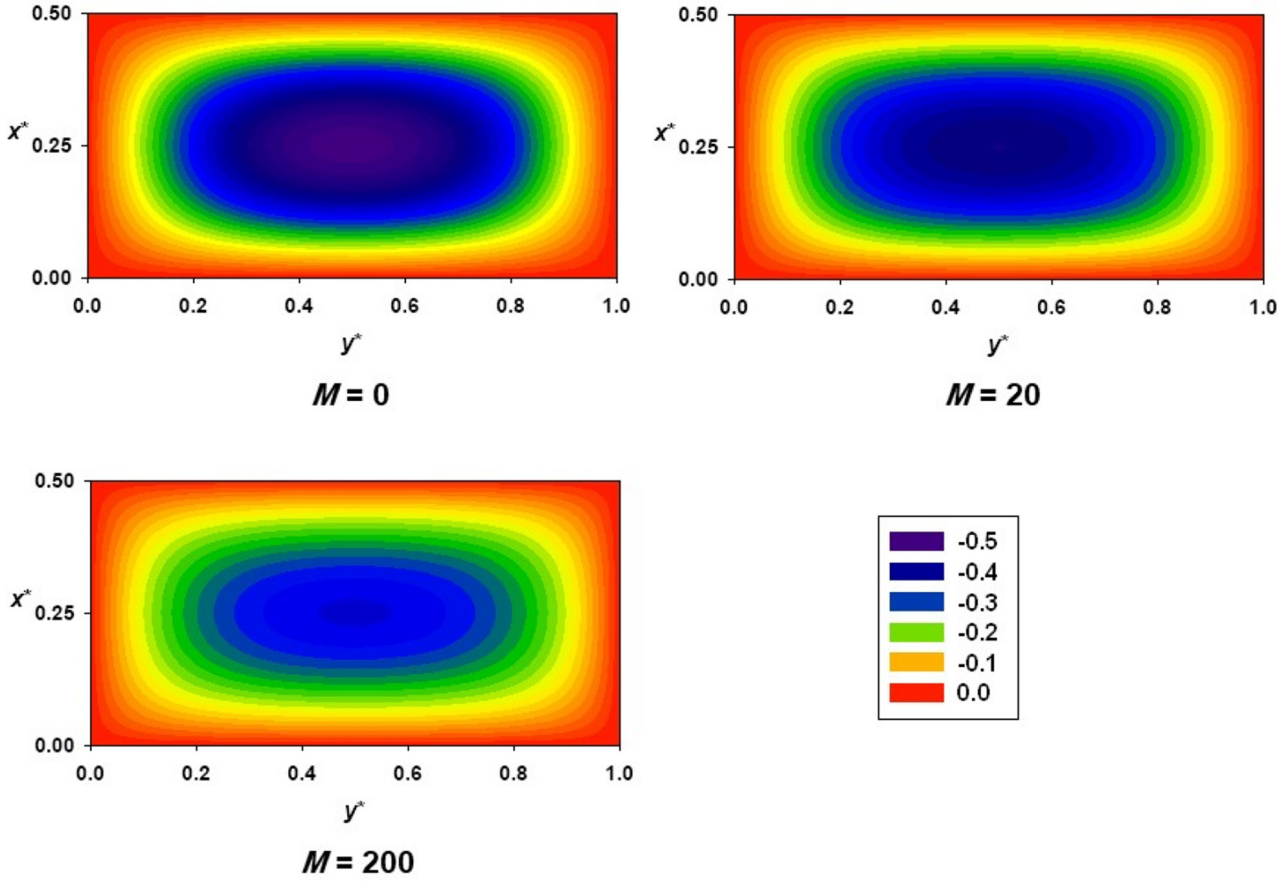

Fig. 16. Dimensionless temperature contours are shown in color bands for $r = 0.5$ and different Hartmann numbers with uniform surface heat flux boundary condition.

rectangular shapes. From previous studies [9–11,21], for square and circular ducts, it was shown that the effect of the magnetic field is to increase the pressure drop in the flow. Fig. 19 shows this reality for any cross-sectional shape except for low M and high r. The curves for $M = 0$ and 10 and for $r > 8$ will coincide but for higher Hartmann numbers, the pressure drop will be lower at $r = 10$ from that at $r = 0.1$ since the short side of r = 10 is exposed to magnetic field, in contrast to that one for $r = 0.1$ where the long side is exposed to the field. Thus, the influence of the field on the former case is less and this is shown in Fig. 19.

The effect of r and M on the heat transfer is illustrated in Figs. 20 and 21 for both thermal boundary conditions; uniform surface temperature and constant surface heat flux, respectively. As the case for the pressure drop, the Nusselt number is plotted versus the aspect ratio for different Hartmann numbers. Again, from the previous work [9,10,21] for square and circular duct, it was proved that the magnetic field will increase the Nusselt number since the temperature distribution will be more homogeneous over the cross section of the duct. However, in general, it will not be true for aspect ratios larger than 4 and at Hartmann number less than 100, as shown in Fig. 20, but eventually the Nusselt number will be inversely proportional to Hartmann number in that region, for the same reason discussed above when the reversal behavior is occurred on the temperature distribution for constant surface temperature. In the case of uniform surface heat

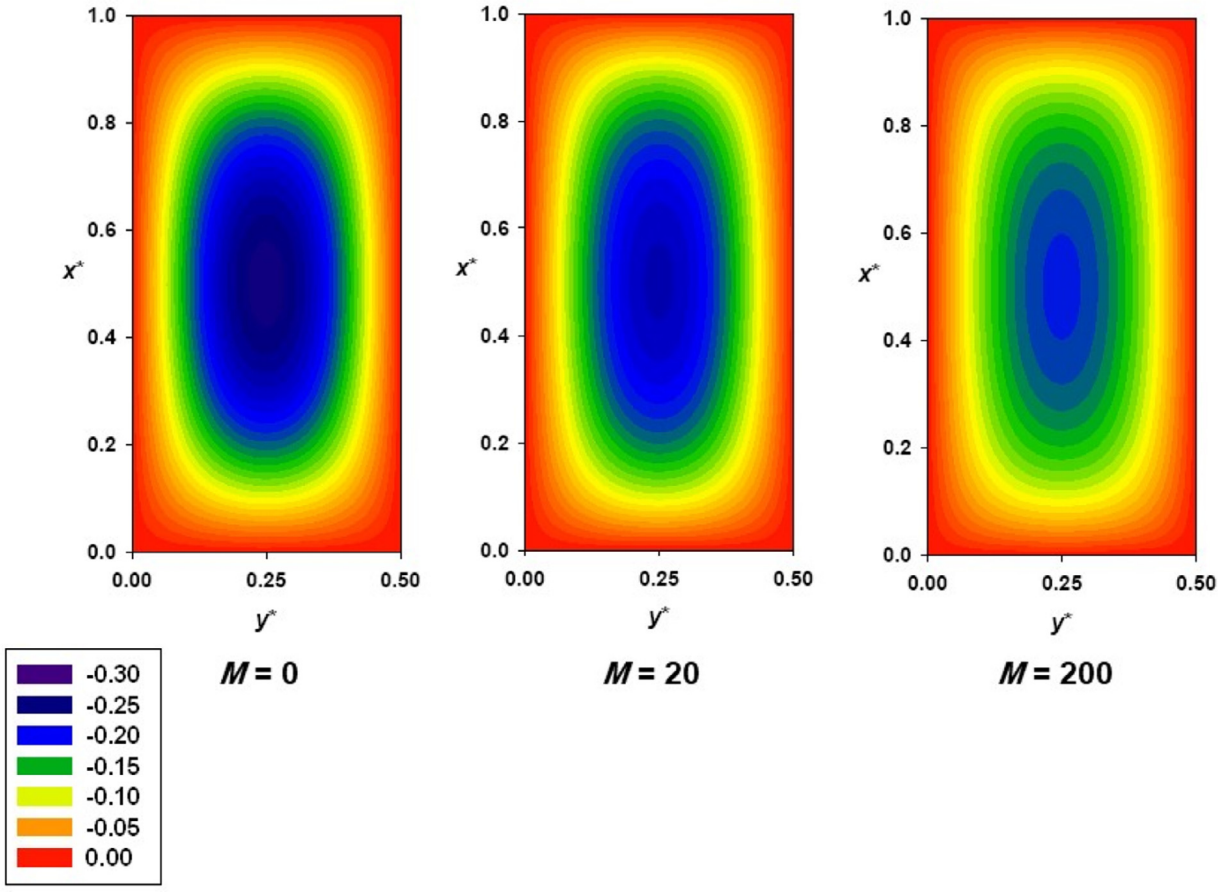

Fig. 17. Dimensionless temperature contours are shown in color bands for $r = 2$ and different Hartmann numbers with uniform surface heat flux boundary condition.

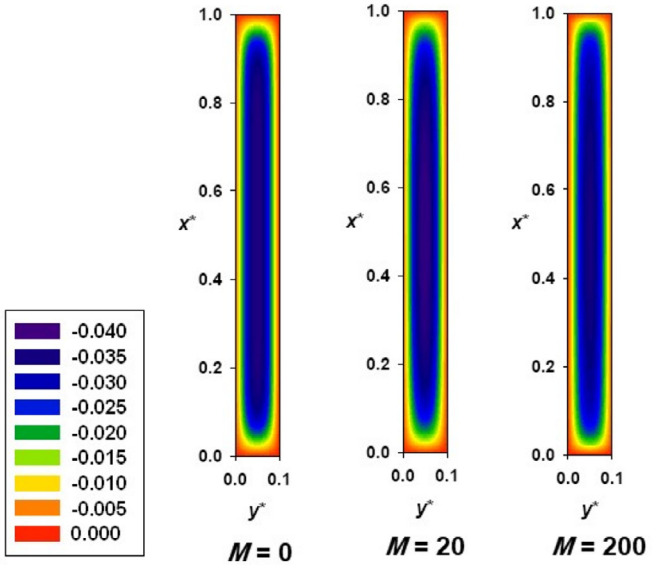

Fig. 18. Dimensionless temperature contours are shown in color bands for $r = 10$ and different Hartmann numbers with uniform surface heat flux boundary condition.

flux, this behavior will be noticed only at $r > 4$ and $M < 10$ since in this case the temperature distribution more uniform than the former one. Also, we can notice from Figs. 20 and 21 that the symmetry from $M = 0$ about $r = 1$ is destroyed due to the effect of the magnetic field.

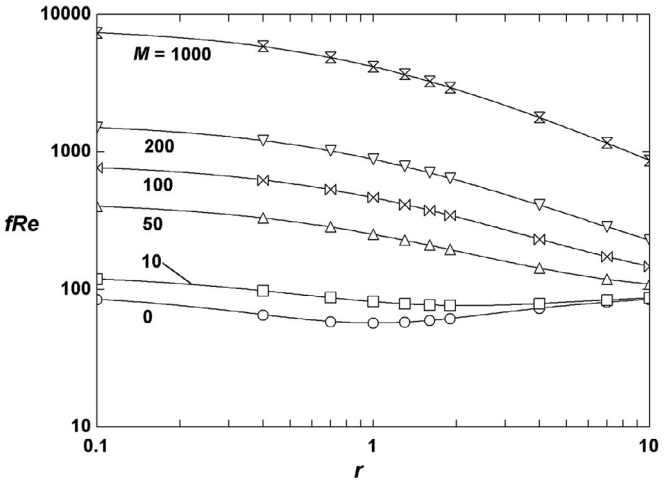

Fig. 19. Friction factor as a function of r for different Hartmann numbers.

5. Conclusion

It is very interesting to notice that the pressure drop and heat transfer are affected by the magnetic field and as well as aspect ratios. For $r = 10$ and $M = 0$, it was shown that the velocity profile along x direction is flatter than y direction due the viscous effects. However, when the field is turned on, the profile will be flattened but with less effect along y direction, whereas the profile will be mostly affected for high M and at $r = 0.1$. Without the field, the pressure drop will be

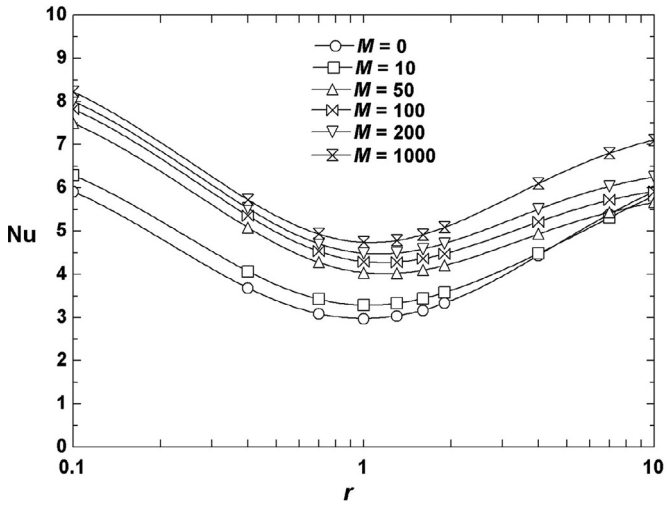

Fig. 20. Nusselt number as a function of r for different Hartmann numbers with uniform surface temperature boundary condition.

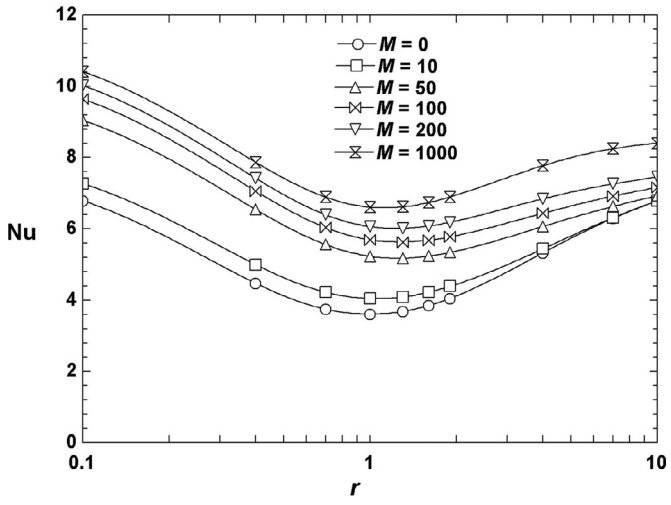

Fig. 21. Nusselt number as a function of r for different Hartmann numbers with uniform surface heat flux boundary condition.

the lowest, but as M increases, the friction factor will increase as expected, except for low M and high r.

In general, the uniformity of the temperature distribution over the cross section with M will increase from $r = 0.1$ to 1 for both thermal boundary conditions (constant surface temperature and uniform heat flux), but after 2 the reversal effect will take place, particularly for constant surface temperature boundary condition. Also, the reversal behavior for Nu is seen here. For $r > 4$ and $M < 100$, Nu decreases for uniform surface temperature boundary condition, but this reverse will be less noticeable for constant wall heat flux boundary condition at $r > 4$ and $M < 10$.

As future work, one can modify the problem to include a non-uniform magnetic field along the duct or be positioned in different angles for fully developed and/or developing flow steady and unsteady flow conditions. The addition of turbulent fluctuations is also interesting. Dealing with turbulence is not easy task because it requires a special turbulence modeling. In order to predict turbulent flows by numerical solutions to Navier-Stokes equations, it becomes necessary to make closing assumptions about the apparent turbulent stress and heat flux quantities. It is important to remember that turbulence models must be verified by comparing predictions with experimental measurements.

Declaration of Competing Interest

The authors declare that they have no known competing financial interests or personal relationships that could have appeared to influence the work reported in this paper.

Acknowledgments

Open Access funding provided by the Qatar National Library.

References

[1] Mohamed E. Sayed-Ahmed, Hazem A. Attia, MHD flow and heat transfer in a rectangular duct with temperature dependent viscosity and Hall effect, Int. Commun. Heat Mass Transf. 27 (8) (2000) 1177–1187.
[2] S.Yu. Smolentsev, A.V. Tananaev1, D.A. Dajeh, Laminar heat transfer in MHD-flow in a rectangular duct. 1. Numerical and analytical studies, Magnetohydrodynamics 33 (2) (1997) 1487-1154.
[3] S.Yu. Smolentsev, A.V. Tananaev1, D.A. Dajeh, V.S. Shmarov, Laminar heat transfer in MHD-flow in a rectangular duct. 2. Experimental studies, Magnetohydrodynamics 33 (2) (1997) 155–160.
[4] K.S. Sai, B.N. Rao, Magnetohydrodynamic flow in a rectangular duct with suction and injection, Acta Mech 140 (1-2) (2000) 57–64.
[5] S.L.L. Verardi, J.R. Cardoso, M.C. Costa, Three-dimensional finite element analysis of MHD duct flow by the penalty function formulation, IEEE Trans. Magn 37 (2001) 3384–3387 5, Sep.
[6] H. Kumamaau, S. Kodama, H. Hirano, K. Itoh, Three-dimensional numerical calculations on liquid-metal magnetohydrodynamic flow in magnetic-field inlet-region, J Nucl Sci Technol 41 (5) (2004) 624–631.
[7] A.I. Nesliturk, M. Tezer-Sezgin, Finite element method solution of electrically driven magnetohydrodynamic flow, J. Comput. Appl. Math. 192 (2) (2006) 339–352.
[8] M. Tezer-Sezgin, C. Bozkaya, Fundamental solution for coupled magnetohydrodynamic flow equations, J. Comput. Appl. Math. 203 (1) (2007) 125–144.
[9] Mohammed J. Al-Khawaja, Mohamed Selmi, "Highly accurate solution of a laminar square duct flow in a transverse magnetic field with heat transfer using spectral method, J Heat Transfer 128 (2006) 413–417.
[10] M.J. Al-Khawaja, R.K. Agarwal, R.A. Gardner, Numerical study of magneto-fluid-mechanic combined free-and-forced convection heat transfer, Int. J. Heat Mass Transf. 42 (1999) 467–475.
[11] F.-C. Li, D. Sutevski, S. Smolentsev, M. Abdou, Experimental and numerical studies of pressure drop in PbLi flows in a circular duct under non-uniform transverse magnetic field, Fusion Eng. Des 88 (2013) 3060–3071.
[12] Dipjyoti Sarma, P.N. Deka, Study on liquid Metal MHD flow through a triangular duct under the action of very strong transverse magnetic field, Int. J. Math. Anal. 5 (5) (2014).
[13] Dmitry Krasnov, Oleg Zikanov, Thomas Boeck, Numerical study of magnetohydrodynamic duct flow at high Reynolds and Hartmann numbers, J. Fluid Mech 704 (2012) 421–446.
[14] Ibrahim Çelik, Solution of Magnetohydrodynamic flow in a rectangular duct by Chebyshev Polynomial Method, Appl. Math. 2 (3) (2012) 58–65.
[15] Xuan Zhang and Oleg Zikanov, "Mixed convection in a downward flow in a vertical duct with strong transverse magnetic field", APS/123-QED, 2018, DOI: 10.1063/1.5048286.
[16] C.N. Kim, Numerical analysis of a magnetohydrodynamic duct flow with flow channel insert under a non-uniform magnetic field, J Hydrodynam B 30 (2018) 1134–1142.
[17] Elif Ebren Kaya, Münevver Tezer-Sezgin, The BEM Solutions of MHD Flow and Heat Transfer in a Rectangular Duct with Temperature Dependent Viscosity, Eur. J. Comput. Mech. 28 (Issues 1-2) (2018) 97–122.
[18] Münevver TEZER-SEZGİN, Merve GÜRBÜZ, Numerical solution and stability analysis of transient MHD duct flow, J. BAUN Inst. Sci. Technol. 20 (3) (2018) 53–61 Special Issue.
[19] Sultan Z. Alamria, Ambreen A. Khan, Mariam Azeez, R. Ellahi, Effects of mass transfer on MHD second grade fluid towards stretching cylinder: a novel perspective of Cattaneo–Christov heat flux model, Phys. Lett. A 383 (Issues 2-3) (2019) 276–281.
[20] Z.H. Khan, O.D. Makinde, M. Hamid, Rizwan Ul Haq, W.A. Khan, Hydromagnetic flow of ferrofluid in an enclosed partially heated trapezoidal cavity filled with a porous medium, J. Magn. Magn. Mater. 499 (2020) Article 166241.
[21] Mohammed J. Al-Khawaja, Mohammed Selmi, Numerical solutions of two heat transfer limits of mfm square duct flow using MatLab program, Int J Comput Meth Eng Sci Mech 10 (1) (2009) 102–107.
[22] Dipjyoti Sarma, G.C. Hazarika, P.N. Deka, Numerical study of liquid metal MHD Flow through a square duct under the action of strong transverse magnetic field, Int. J. Comput. Appl. 71 (8) (2013).